Ion irradiation induced effects in silica glasses

Teun van Dillen

FOM-Institute for Atomic and Molecular Physics
Kruislaan 407, 1098 SJ, Amsterdam
The Netherlands

Master thesis for the study experimental physics at Utrecht University
February 1998 – April 1999

Supervisors: Dr. E. Snoeks, Dr. Ir. M.L. Brongersma,
Dr. A. van Blaaderen and Prof. Dr. A. Polman

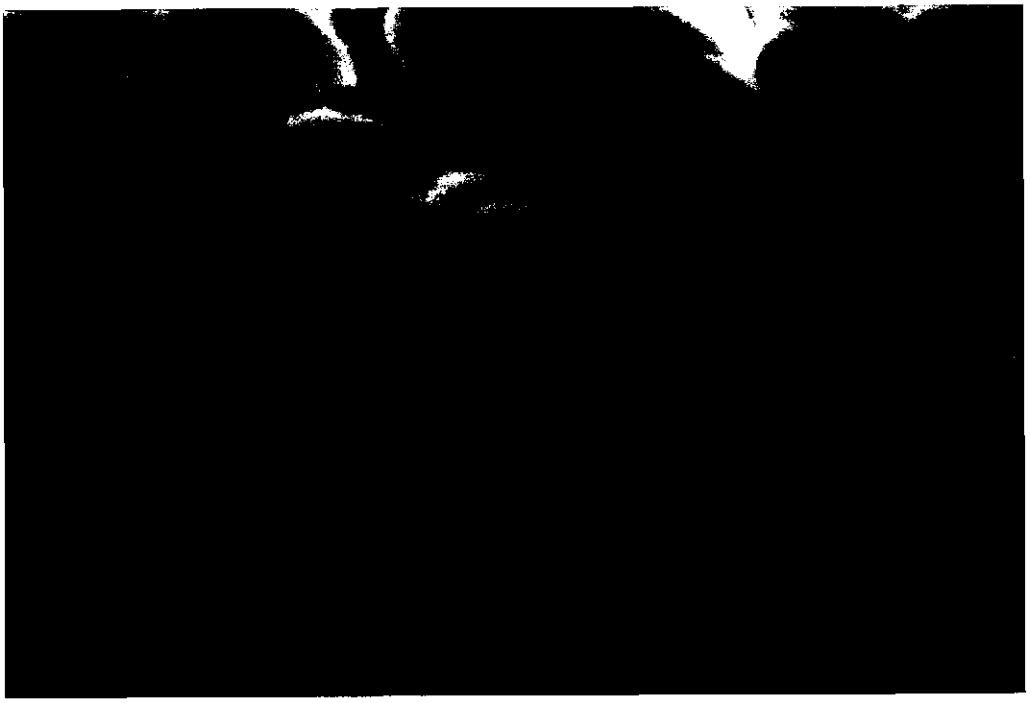

AMOLF FOM

Dankwoord

Ongeveer anderhalf jaar geleden ben ik met een excursie naar het FOM Instituut voor Atoom –en Molecuulfysica, het Amolf meegeweest. Het was onderdeel van het vak Materiaal Onderzoek op Atomaire Schaal (MOAS). Dit keuzevak, dat ik als student experimentele natuurkunde aan de Universiteit van Utrecht volgde, werd gegeven door prof. dr. Albert Polman, tevens groepsleider van de groep 'opto-electronische materialen'. Ik had veel geluk want ik kon in zijn groep aan de slag gaan als stagiair met niet één, niet twee maar drie begeleiders: Mark Brongersma, Edwin Snoeks en Albert Polman.

Het jaar verliep zeer succesvol. Een hoogtepunt, naar mijn mening, was de internationale conferentie IBMM (Ion beam modification of materials) in Amsterdam, georganiseerd door onze groep. Ik heb daar de kans gekregen om mijn werk te presenteren in de vorm van een poster. Het was een unieke ervaring om met verschillende mensen uit hetzelfde vakgebied over mijn onderzoek te discussiëren. Tevens heb ik een artikel geschreven voor de proceedings van deze conferentie. Een tweede hoogtepunt volgde al snel. Naast het onderzoek waar ik oorspronkelijk mee was begonnen, werd ik betrokken bij het onderzoek aan het vervormen van silica balletjes. Met Alfons van Blaaderen als vierde begeleider heb ik aan dit onderzoek gewerkt. Concluderend was het dus een leerzaam jaar waarin ik meer heb gedaan dan onderzoek alleen.

Als eerste wil ik Albert bedanken. Jij hebt me de kans gegeven om onderzoek te doen in jouw groep. We kunnen terugkijken op een gezellig en produktief jaar. Van onze gesprekken heb ik veel geleerd. Je hebt mijn enthousiasme voor natuurkundig onderzoek gestimuleerd en ik ben je heel dankbaar voor de kans die ik krijg om als OIO in jouw groep door te gaan.

Ten tweede wil ik Mark, Edwin en Alfons bedanken voor hun begeleiding. Jullie hebben me steeds nieuwe inzichten gegeven en van jullie enthousiasme en creativiteit heb ik heel veel geleerd. Ik kan zonder twijfel zeggen dat ik me geen betere begeleiders had kunnen voorstellen.

Naast mijn vaste begeiders bedank ik uiteraard ook de overige groepsleden: Michiel de Dood, Lenneke Slooff, Pieter Kik, Christof Strohhöfer, Dirk Vossen, Michael Hensen en Jan van der Elsken. Ik wil ook graag een aantal oud-groepsleden bedanken: Nicolas Hamelin, José dos Santos, Daniel Peters en Freek Suyver. De samenwerking binnen de groep is uniek en heeft mij altijd gestimuleerd. Van onze werkbesprekingen heb ik veel geleerd.

Ik wil bij deze ook een woord van dank wijden aan onze groepstechnici Johan Derks en Jan ter Beek. Dankzij jullie zijn de apparaten continu in bedrijf en kunnen wij in een snel tempo ons onderzoek doen.

Tot slot wil ik graag mijn familie bedanken. Mijn ouders en mijn broer wil ik bedanken voor hun liefdevolle steun. Dag in, dag uit stonden jullie voor me klaar. Zonder jullie steun en enthousiasme was ik nooit zo ver gekomen.

Teun van Dillen, April 1999

Table of Contents

The results reported in this master thesis are also reported in:

- T. van Dillen, M.L. Brongersma, E. Snoeks, A. Polman, Nucl. Inst. Meth. B **148**, 221 (1999)
- M.L. Brongersma, E. Snoeks, T. van Dillen, and A. Polman, submitted to J. Appl. Phys.
- E. Snoeks, A. van Blaaderen, C.M. van Kats, M.L. Brongersma, T. van Dillen and A. Polman, submitted to Science

1. Introduction

Ion implantation is a frequently used technique in today's physical research. This technique is applied in materials science, for example in the field of opto-electronics and semiconductor physics. During ion implantation every ion penetrating a material loses energy by atomic collisions and electronic excitations, which changes the properties of the irradiated material. Ion irradiation induced effects in a wide class of materials have been studied for many years. Examples of these effects are defect generation and annihilation, structural transformations, viscous flow and anisotropic deformation [1, 2, 3].

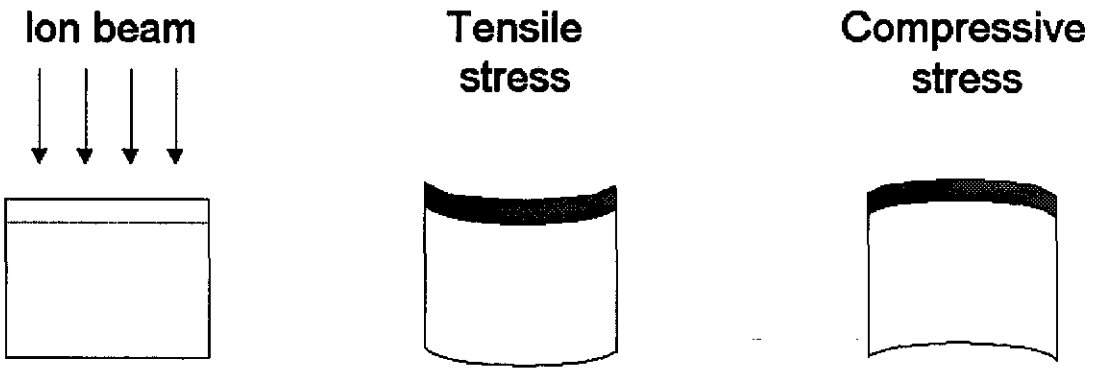

Figure 1.1 Possible effects of ion irradiation of bulk samples or thin films constrained by a substrate. If the ion modified film wants to contract a tensile stress is built up. An expansion of the film leads to a compressive stress.

Ion irradiation induced phenomena can be studied by measuring the mechanical stress in the ion modified film or by measuring the deformation of the ion irradiated material. If, for example, we irradiate a freestanding object, the material is free to expand or contract in any direction. If, however, the irradiated material is constrained by a substrate this might lead to the build-up of mechanical stress. An example is schematically depicted in Fig. 1.1, where a thick bulk sample is irradiated with ions. Due to nuclear and electronic stopping the ions have a range much smaller than the thickness of the sample. Therefore only the top film of this sample is modified. As a result of this ion beam modification this thin film might want to contract. In this case the thin film is under a tensile stress, because it is constrained by the substrate, the non-irradiated part of the sample. If the thin film wants to expand, a compressive stress is built up. In both cases the build-up of stress is accompanied by a curvature of the sample which can be measured.

In this master thesis we apply MeV Xe ion irradiation to investigate ion beam induced effects. One way of doing this is by measuring the curvature of a sample during and after ion irradiation (Fig. 1.1). In chapter 2 we describe the setup used to in-situ measure the curvature of a sample. In chapter 3 we apply this technique to study ion irradiation-induced defects and viscous flow. In chapter 4 this technique will be used to investigate anisotropic stress generation. Finally, in chapter 5 we apply the ion irradiation technique to deform micron-sized silica colloids into oblate and prolate spheriods. In this case the deformation of these colloids is investigated by scanning electron microscopy (SEM).

2. Experimental setup

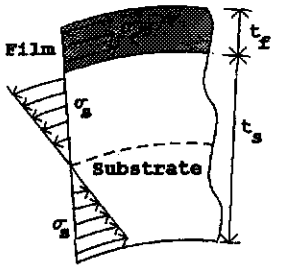

Figure 2.1 Schematic diagram of the stress distribution in a thin film (thickness t_f) and the substrate (thickness t_s).

In chapter 1 it was already discussed that ion irradiation can bring about mechanical stress in a sample. The in-plane stress σ is defined to be the force per unit area parallel to the surface normal.

Figure 2.1 shows a schematic diagram of a thin film (ion modified region, thickness t_f) constrained by a substrate (thickness t_s). The stress distribution in the film (σ_f) and in the substrate (σ_s) are also shown in this figure [4]. In this report we are concerned with determining the stress σ_f in the thin film. If we assume that the film thickness is much smaller than the substrate thickness, the average in-plane stress σ_f in the film can be calculated from the curvature R of the sample, by using Stoney's equation [4,5]:

$$\sigma_f = \frac{Y_{b,s} \cdot t_s^{\,2}}{6Rt_f} \,. \tag{2.1}$$

$Y_{b,s}$ is the biaxial modulus of the substrate given by $Y_s/(1-\nu_s)$, where Y_s and ν_s are Young's modulus and the Poisson's ratio, respectively.

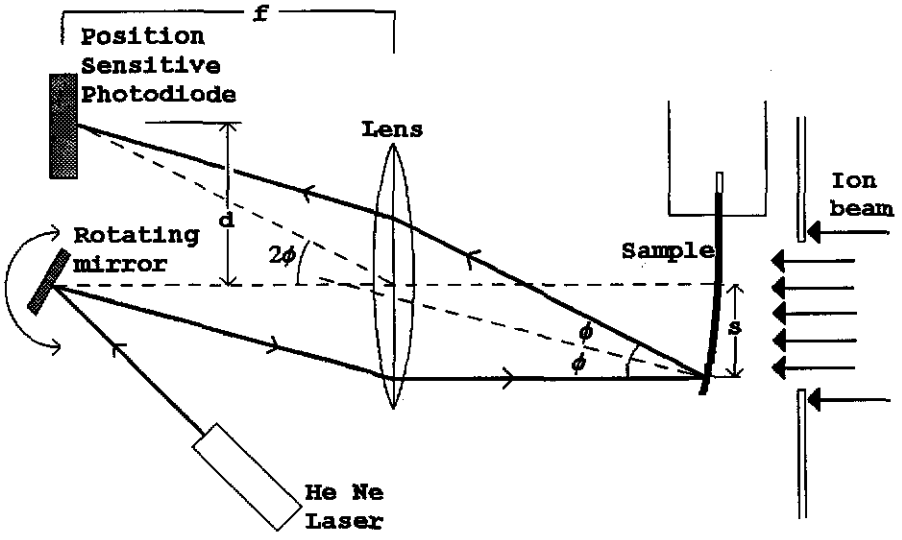

Figure 2.2 Schematic illustration of the wafer curvature setup. This setup is used to measure the radius of curvature R of a sample during and after ion implantation

The setup used to measure the radius of curvature of the sample during and after ion implantation is schematically depicted in figure 2.2 and was built based on a description described in Ref. [6]. One end of a sample is clamped to a temperature controlled block leaving the other end free to bend. One side of the sample is homogeneously irradiated with an ion beam. The sample curvature is measured by a sensitive scanning-laser technique described below.

A He Ne laser beam is reflected by a galvanometer-controlled, rotating mirror set in the focal plane of a 1 m converging lens. After passing through the lens the scanning laser beam is therefore parallel to the optical axis. The beam is then reflected off the back surface of the sample and after passing through the same lens the beam falls onto a position sensitive photodiode which is also placed exactly in the focal

plane of the mirror. During the laser scan the position d of the reflected beam on the detector is linearly related to the angle ϕ between the incoming laser beam and the surface normal of the sample at that point, provided that ϕ is small. From figure 2.2 we derive:

$$d = f \tan(2\phi) \approx 2f\phi \ , \tag{2.2}$$

where f is the focal length of the converging lens (1m). A change Δd in the detector position as the beam is scanned Δs along the sample is:

$$\frac{\Delta d}{\Delta s} = 2f \frac{\Delta \phi}{\Delta s} = \frac{2f}{R} \ , \tag{2.3}$$

where R is the radius of curvature of the sample at point s (Fig. 2.2). From Eq. (2.3) we can conclude that the laser spot remains stationary(Δd=0) in case of a flat sample (R=∞). The position and intensity of the laser spot on the photodiode were recorded by a computer; Eq. (2.3) was used to determine the curvature R of the sample from the recorded data. More details are described in [6, 7]. Using Stoney's equation (2.1) the average in-plane stress in the ion modified region can be calculated.

3. Activation energy spectra for annealing of ion irradiation induced defects in silica glasses

3.1 Introduction

The effect of ion irradiation on the structure of silica glasses has been studied for many years, and many of the radiation-induced phenomena that can occur are now well established. For example, ion irradiation can cause structural transformations in which rearrangements in the glass network topology take place [2]. When the irradiated region is constricted by a substrate, such changes may lead to the build-up of mechanical stress in the material. This stress can be relaxed by radiation-induced viscous flow [1, 8]. In addition, irradiation at high (MeV) energies may cause anisotropic deformation, leading to stress in the plane perpendicular to the direction of the ion beam [1, 3, 9, 10]. This ion irradiation phenomenon will be described in more detail in chapters 4 and 5.

Ion irradiation also leads to the generation of point defects or larger defect agglomerates. Spectroscopic techniques have been used to try to identify the charge state and bonding nature of these defects [2, 11]. Little is known, however, about the typical annihilation activation energies of these defects and their steady state concentration as a function of activation energy. One way to study this is by measuring the mechanical stress in an irradiated region that has built up due to the excess volume generated by such defects [1]. In this chapter, we present stress measurements during and after 2 MeV Xe ion irradiation of alkali-borosilicate glass and SiO_2 films, thermally grown on Si. Measurements are performed at different irradiation temperatures in the range from 95-580 K. The results are compared with similar measurements that were recently performed on 4 MeV Xe irradiated thermally grown SiO_2 films [8, 12]. Some striking differences between the defect spectra are found, and are related to a fundamental difference in the nature of the defect generation process.

3.2 Experimental

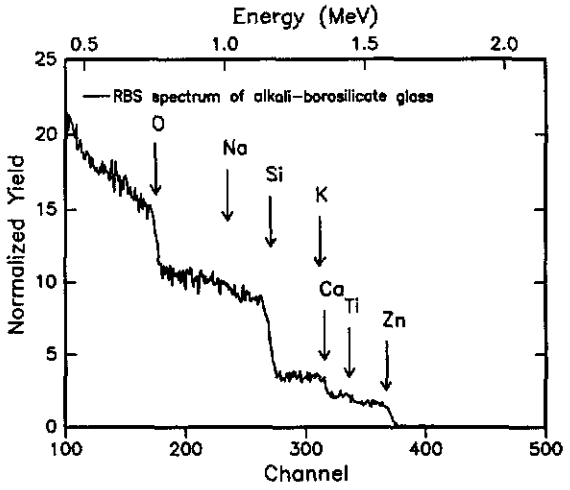

Figure 3.1 RBS spectrum of alkali-borosilicate glass, performed with 2.0 MeV $^4He^+$.

Measurements were performed on 150 μm thick rectangular bulk alkali-borosilicate glass samples (6x23 mm^2, Menzel cover glasses). Figure 3.1 shows the Rutherford backscattering spectrometry (RBS) spectrum of this glass. It contains (besides Si and O) approximately 4.7 at% Na and also small concentrations of K, Ca, Ti and Zn. Elastic Recoil Detection (ERD) measurements show that this glass contains about 3.7 at% B. One end of the samples was clamped to a temperature-controlled copper block, leaving the other end free to bend. The bare glass-side of the samples was homogeneously irradiated with a 2 MeV Xe ion beam that was electrostatically scanned over the sample with an ion flux of 4-9×10^{10} ions/cm^2s. The maximum ion range was about 1.0 μm [1]. During irradiation the radius of curvature of the sample was measured using a sensitive scanning laser technique, from which the average in-plane stress σ in the irradiated region was derived (see chapter 2). In order to obtain a good reflection from the sample a 50 nm thick Cr film was evaporated on the backside of the sample. The measurements were performed at fixed temperatures between 95 and 580 K.

In addition, measurements were performed on 2.4 μm thick SiO_2 films grown by wet thermal oxidation (1100 °C) on 95 μm thick Si (100) substrates. These films were homogeneously irradiated with 2 MeV Xe ion beam at a flux of 1-1.5×10^{11} ions/cm^2s at fixed sample temperatures between 90 and 375 K.

3.3 Results and analysis

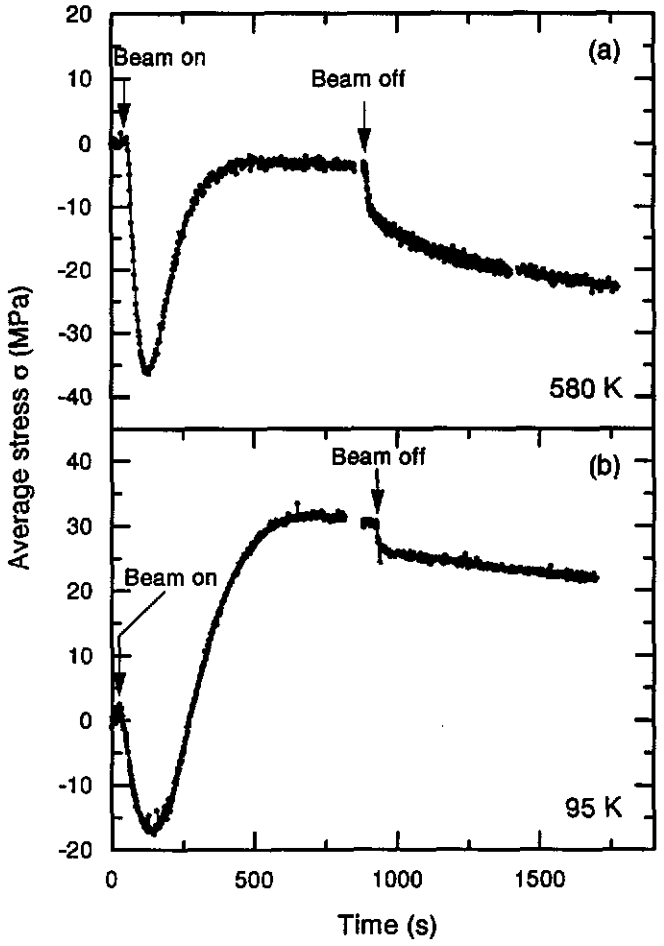

Figure 3.2 In-situ measurements of the average in-plane stress σ of alkali-borosilicate glass before, during and after 2 MeV Xe irradiation as a function of time. Results are shown for a sample temperature of 580 K (a), and 95 K (b). The ion beam was switched off after a total irradiation fluence of 8×10^{13} Xe/cm^2 (a), 4.3×10^{13} Xe/cm^2 (b).

We will first describe the data measured on the alkali-borosilicate glass samples. Figure 3.2(a) shows a typical stress measurement as a function of time during and after ion irradiation at a temperature of 580 K. The ion beam is switched on at t=54 s and switched off at t=893 s. In this report, compressive stress is defined to be positive. After switching on the ion beam there is small initial increase in the stress. The stress then becomes tensile and reaches a maximum tensile stress at t=130 s, corresponding to a Xe fluence of 7.3×10^{12} cm^{-2}. The stress then turns towards compressive values and saturates at a value of –3 MPa after ~500 s, corresponding to a fluence of about 4×10^{13} Xe cm^{-2}.

As shown previously, the stress changes during ion irradiation are caused by different processes that occur simultaneously [8, 12]. The small initial peak is caused by stress induced by the creation of volume occupying defects in the glass as the ion beam is switched on. The subsequent change towards tensile stress is attributed to a structural change of the glass [12]. At the same time, radiation-induced viscous flow occurs, a continuous stress-driven process that eventually relaxes the stress towards zero. Figure 3.2(b) shows a stress measurement at a temperature of 95 K. It shows the same features as the data in Fig. 3.2(a), except that the stress saturates at a positive value. As described earlier, this is due to an anisotropic stress generation phenomenon in the silica glass, that occurs at low temperature [1, 3, 9, 10] (see chapter 4).

After switching off the ion beam the stress changes towards tensile values as can be seen in Fig. 3.2 both at 95 K and 580 K. The same effect was also observed in measurements performed at intermediate temperatures [13]. This stress change is attributed to the annealing of volume occupying defects (generated by the ion beam) that have a spectrum of annealing times. The densification is given by (see appendix) [12]:

$$\Delta\rho = \Delta\rho_\infty - \int_0^\infty D(Q)\cdot e^{-t'/\tau(Q)}dQ\,, \tag{3.1}$$

where $D(Q)$ is the density change per unit energy, t' is time after switching off the beam and $\tau(Q)$, given by:

$$\tau(Q) = \frac{h}{kT}\cdot e^{Q/kT}\,, \tag{3.2}$$

is the characteristic annealing time of defects with an activation energy Q. In Eq. (3.2) k and h are Boltzmann's and Planck's constants respectively and T is the temperature.

If the activation energy spectrum of the defects is very broad and varies slowly with activation energy it follows from Eq. (3.2) that at a time t' after switching off the ion beam defects with activation energies in a small band of order kT around

$$Q_{t'} = kT \cdot \ln(t' \cdot kT / h) , \tag{3.3}$$

are annealing out, resulting in a certain stress change. The spectrum $D(Q_t)$ can then be approximated from the measured stress change by [12] (more details in appendix):

$$D(Q) = \frac{-3\rho}{kT \cdot Y_b} \cdot \frac{d(\Delta\sigma)}{d\left(\ln[t' \cdot kT / h]\right)} , \tag{3.4}$$

where $\Delta\sigma$ is the stress change after switching off the ion beam with respect to the saturation stress, ρ is the density of the silica glass (6.9×10^{22} atoms/cm^3) and Y_b the biaxial modulus of the modified region of the glass (90 GPa) [1].

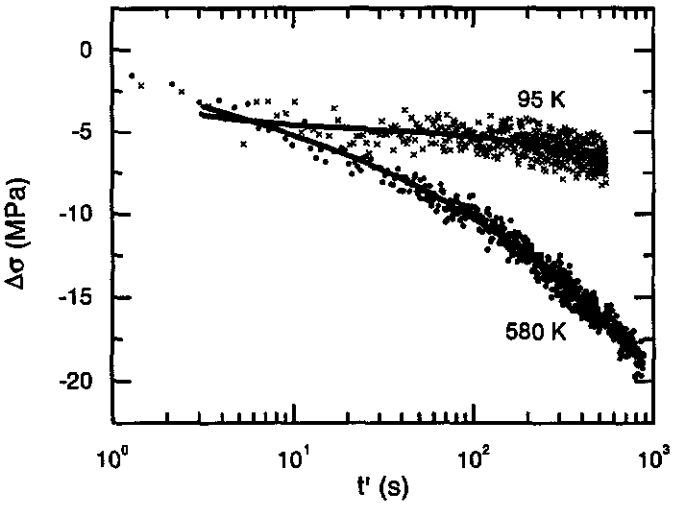

Figure 3.3 The stress change $\Delta\sigma$ from Fig. 3.2 (relative to saturation stress) after switching off the ion beam, plotted as a function of the time after switching off the ion beam (t'). Results are shown for the alkali-borosilicate glass at sample temperatures of 580 and 95 K (from Fig. 3.2). At both temperatures the samples were first irradiated to reach a saturation stress value. The drawn lines are polynomial fits through the data.

Fig. 3.3 shows the transient stress change from Fig. 3.2 after switching off the ion beam on a logarithmic time scale. According to Eq. (3.4) the spectra $D(Q)$ can now be calculated by taking the derivative of $\Delta\sigma$ with respect to $ln(t' \cdot kT/h)$. This is done by fitting a 3rd order polynomial to the data and then taking the derivative of these curves versus $ln(t')$. The result is shown in Fig. 3.4(a), where $D(Q)$ is plotted versus Q for the temperatures between 95 and 580 K. To avoid possible contributions from beam heating on the stress measurement only data for $t'>30$ s are used.

3.4 Discussion

As can be seen in Fig. 3.4(a), at each temperature the spectrum for $D(Q)$ increases with increasing Q over the whole range. It can be seen that at a fixed activation energy the defect density per unit energy decreases with increasing sample temperature.

We will compare these spectra of alkali-borosilicate glass with activation energy spectra derived from stress measurements performed on 2.4 μm thick, thermally grown SiO_2 films on Si [12], that are shown in Fig. 3.4(b). These measurements were done with a 4 MeV Xe^{4+} beam at an ion flux of 5×10^{12} Xe/cm^{2}s and some of them are shown in Fig. 3.5.

In contrast to the case of alkali-borosilicate glass, for SiO_2 no stress change due to defect annealing was observed for temperatures higher than 255 K. Therefore the annihilation activation energy spectrum calculated from the data shows no contributions for $Q > 0.75$ eV as can be seen in Fig 3.4(b). Furthermore, all spectra decrease gradually as a function of the activation energy Q. By comparing all spectra for pure silica measured at different temperatures they seem to fit one 'universal' continuous spectrum. To confirm this, a smooth curve $D(Q)$ was fitted to the spectra of Fig. 3.4(b) (drawn line). The

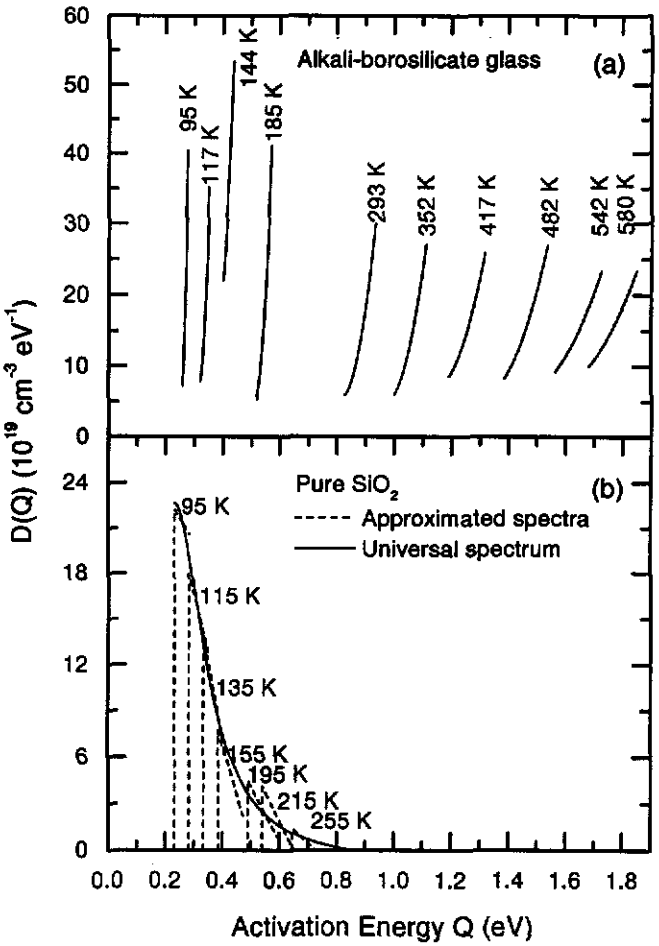

Figure 3.4 (a) Defect annihilation activation energy spectra for alkali-borosilicate glass derived from the data in Fig. 3.3 and from additional data taken at other temperatures (all after irradiation with 2 MeV Xe at a flux of 4-9×10^{10} ions/cm^{2}s). (b) The same for thermally grown SiO_2 films on Si (after irradiation with 4 MeV Xe at a flux of 5×10^{12} ions/cm^{2}s).

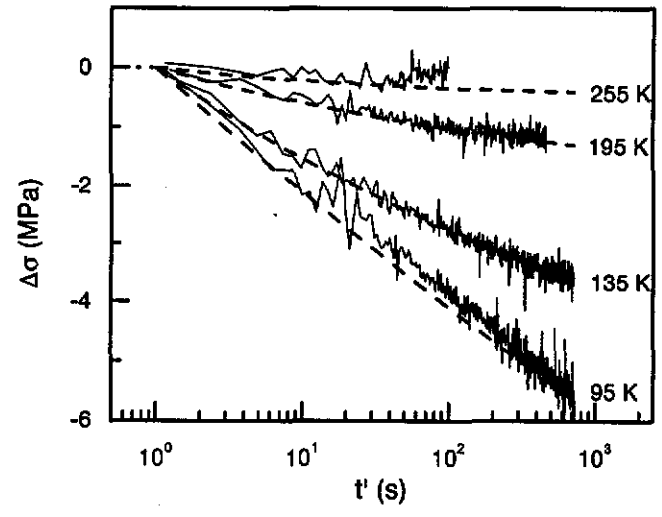

Figure 3.5 The average in-plane stress change in the SiO_2 film after the 4 MeV Xe ion beam was switched off. Results are shown for four sample temperatures 95, 135, 195 and 255 K. The dashed lines are calculations of these stress changes using the universal spectrum in Fig 3.4 and Eq. (3.1)

time dependence of the stress change was then calculated using this spectrum and Eq. (3.1), and the result is shown for four temperatures in Fig. (3.5). Good agreement with the measured data is observed. Comparing the spectra of the two glass types it can first be concluded that defects are more stable in alkali-borosilicate glass, because the spectrum for alkali-borosilicate glass has non-zero values up to at least 1.85 eV whereas for the thermal oxide the spectrum vanishes above 0.75 eV.

The universal behavior of the spectra for thermal SiO_2 can be explained using a thermal spike model [12]. The defect generation is independent of sample temperature, as the temperature in the thermal spike [8, 12, 14] is much higher than the sample temperature. The defect population that is probed by the stress measurement is generated during the thermal spike that causes local melting of the SiO_2 film, and quenched in during rapid cooling.

The fact that this 'universal' behavior is not found for alkali-borosilicate glass implies that in this glass the steady state concentration of defects depends on sample temperature. This can be explained by a binary collision model for which in contrast to a thermal spike, an ion impact does not cause local melting but produces isolated defects as a result of binary collisions. In this case, a steady state defect population builds up due to a temperature independent defect generation and a temperature dependent defect annihilation. Therefore the steady state defect population then depends on the activation energy Q, the sample temperature and the maximum concentration of defects that can be generated for each Q. Because the annihilation rate (Eq. (3.2)) is larger for higher temperatures, the steady state defect population for a fixed activation energy is smaller for higher temperatures, which is in agreement with the data in Fig. 3.4(a).

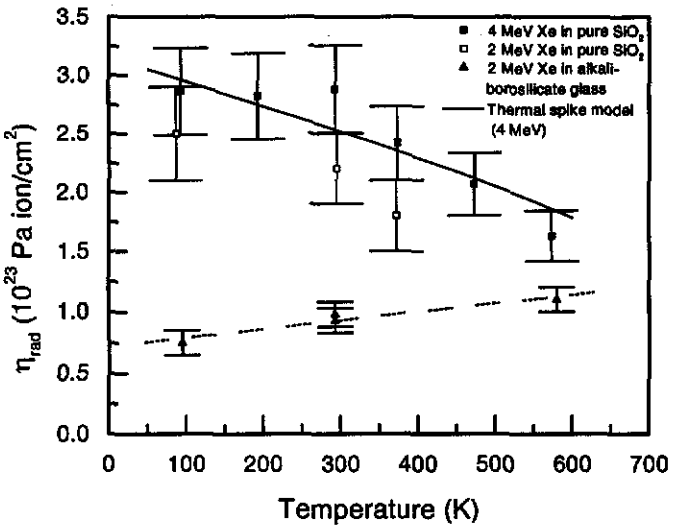

Figure 3.6 The radiation-induced viscosity η_{rad}, derived from stress relaxation data during Xe ion irradiation, plotted as a function of temperature for 2 MeV irradiation of alkali-borosilicate glass (triangles) and 4 MeV irradiation of thermally grown SiO_2 films at a flux of ~10^{11} Xe/cm^{2}s (solid squares). The solid line is a calculation of η_{rad} according to a thermal spike model (multiplied by a factor 4.7 to obtain agreement between the model and the data) [8]. The dashed line is a guide to the eye for the alkali-borosilicate glass. Data for irradiations of thermal SiO_2 using 2 MeV Xe are also shown (open squares).

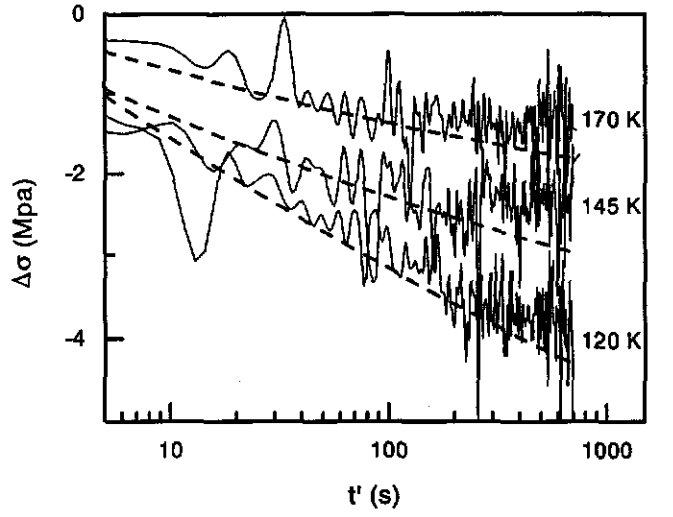

Figure 3.7 The average in-plane stress change in the SiO_2 film after the 2 MeV Xe ion beam (flux: 1-1.5×10^{11} Xe/cm^{2}s) was switched off. Results are shown for three sample temperatures 120, 145 and 170 K. The dashed lines are calculations of these stress changes using the universal spectrum in Fig 3.4 (derived from the 4 MeV Xe irradiations) and Eq. (3.1)

Additional indications for the different nature of the defect generation in the two cases are found by comparing the temperature dependencies of the radiation-induced viscosity η_{rad} [1, 8, 10, 12] for both glass types. These data are derived from stress relaxation measurements during ion irradiation. We estimated η_{rad} by fitting an exponential function to the part of the stress curve (see Fig. (3.2)) between ~ 300 and 700 s (fluence ≳ 1.5×10^{13} Xe/cm^2), the same method as used in [3]. The results are shown in Fig. 3.6. As can be seen, the viscosity for alkali-borosilicate glass (triangles) slowly increases with increasing temperature from (0.75±0.10)×10^{23} Pa ion/cm^2 at 95 K to (1.1±0.10)×10^{23} Pa ion/cm^2 at 580 K. For comparison, the data for pure SiO_2 (solid squares) are included. It is important to note that these data were obtained by using a 4 MeV Xe ion beam, but at a flux of ~10^{11} ions/cm^{2}s (and not 5×10^{12} Xe/cm^{2}s as in Fig 3.4(b) and Fig. 3.5). These show an opposite behavior of η_{rad}, in agreement with calculations using a thermal spike model (the drawn line in Fig. 3.6) [8]. This provides independent evidence that the defect generation in alkali-borosilicate glass is not governed by a thermal spike process.

The different behavior observed above for pure silica and alkali-borosilicate glass may be due to the difference in the ion energy (4 MeV for pure silica versus 2 MeV for alkali-borosilicate glass), the difference in the beam flux that was used (5×10^{12} Xe/cm^{2}s for pure SiO_2 versus 4-9×10^{10} Xe/cm^{2}s for alkali-borosilicate glass), or the difference in the composition of the glass. Indeed it has been shown that the presence of boron affects the stability and the density of ion irradiation induced defects in silica glass [11, 15].

To further investigate the difference in the behavior of defect annealing we also performed relaxation measurements on thermally grown SiO_2 films under the same irradiation conditions as in the case of the alkali-borosilicate glass: 2 MeV Xe at a flux of 1-1.5×10^{11} Xe/cm^{2}s and at different sample temperatures between 95 and 375 K. Fig. 3.7 shows the average in-plane stress change (relative to the saturation stress) after switching off the ion beam after these irradiations. Data are shown for three sample temperatures 120, 145 and 170 K. The time dependence of the stress change was calculated using the same

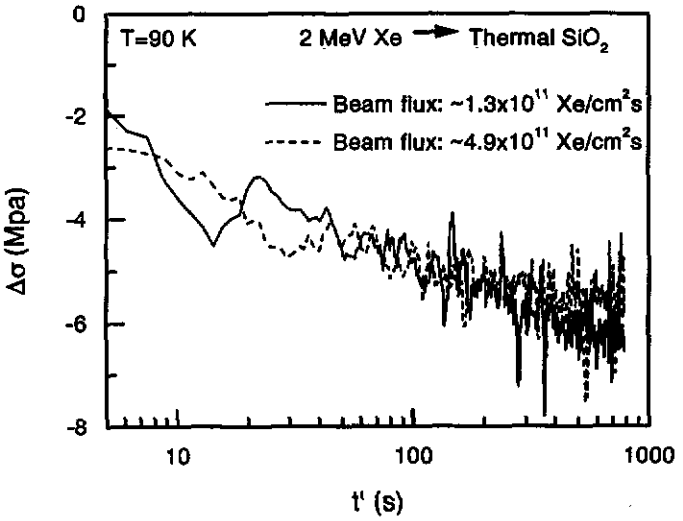

Figure 3.8 The average in-plane stress change in the SiO_2 film after the 2 MeV Xe ion beam was switched off. Results are shown after irradiating with a beam flux of 1.3×10^{11} Xe/cm^{2}s (solid line) and a beam flux of 4.9×10^{11} Xe/cm^{2}s (dashed line). The sample temperature was held constant at 90 K.

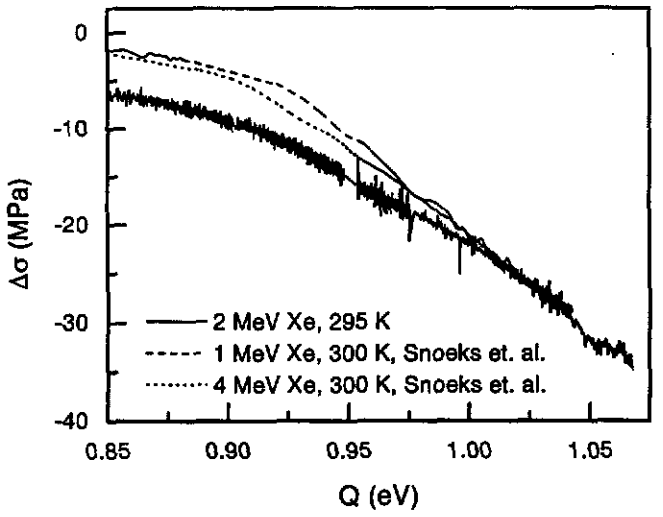

Figure 3.9 The average in-plane stress change in alkali-borosilicate glass after switching off the 2 MeV Xe ion beam (flux: 10^{11} Xe/cm^{2}s) at a sample temperature of 295 K(solid line). Structural relaxation data (taken from reference [1]) after 1 MeV Xe irradiation (dashed line) and after 4 MeV Xe irradiation (dotted line) are also shown. For the latter two curves the temperature was 300 K and the flux during irradiation was ~3×10^{10} Xe/cm^{2}s.

universal spectrum derived from the 4 MeV data (Fig. 3.4(b)) and Eq. (3.1). The result is shown in Fig. 3.7 (dashed lines). Again good agreement with the measured data is observed, indicating that the defect spectrum after 2 MeV Xe irradiation at a flux of about 10^{11} Xe/cm^{2}s is approximately the same as the (universal) spectrum in Fig. 3.4(b). Hence we conclude that the defect activation energy spectrum of thermally grown SiO_2 does not depend on the irradiation energy of the Xe ions in the 2-4 MeV Xe energy range. To study the dependence of the defect spectrum on the beam flux, we raised the beam flux for 2 MeV irradiation of thermal SiO_2 to ~5×10^{11} Xe/cm^{2}s. Experiments performed at a beam flux of ~1.3×10^{11} and ~4.9×10^{11} Xe/cm^{2}s are compared in Fig. 3.8 (solid and dashed line respectively). The sample temperature was 90 K during and after both irradiations. As can be seen no beam flux dependence is found in the structural relaxation behavior.

Next, we investigated the temperature dependence of the radiation-induced viscosity, using a 2 MeV Xe ion beam with a flux of 1-1.5×10^{12} Xe/cm^{2}s. These data are shown in Fig. 3.6 (open squares). The viscosity decreases from $(2.5\pm0.4)\times10^{23}$ Pa ion/cm^2 at 90 K to $(1.8\pm0.3)\times10^{23}$ Pa ion/cm^2 at 375 K. It is seen that the radiation-induced viscosity for 2 MeV irradiation is very similar to that for 4 MeV irradiation (Fig 3.6, closed squares). Similar to the 4 MeV Xe irradiations with a flux of ~10^{11} Xe/cm^{2}s, the radiation-induced viscosity decreases with increasing temperature, consistent with a thermal spike behavior as discussed before.

Finally we investigated the dependence of the structural relaxation behavior of the alkali-borosilicate glass on the energy of the Xe ions. Figure 3.9 shows the average in-plane stress change in alkali-borosilicate glass after switching off a 2 MeV Xe ion beam with a flux of ~10^{11} Xe/cm^{2}s (solid line). The sample temperature was held constant at 295 K. We compared these data with the structural relaxation data of alkali-borosilicate glass presented in [1]. The experiments in [1] were performed at 300 K using a 4 MeV Xe ion beam (dashed line) and a 1 MeV Xe ion beam (dotted line). The beam flux was approximately 3×10^{10} Xe/cm^{2}s. To compare these results taken at slightly different temperatures the stress changes are plotted versus the activation energy Q defined by Eq. (3.3) rather than time. First it can be seen that the slope of all curves in Fig. 3.9 is constant from ~0.96 eV to at least 1.04 eV. For the 2 MeV data this means

that the spectrum rises from 0 to $(35\pm5)\times10^{19}$ cm^{-3} eV^{-1} at ~0.96 eV (like in Fig 3.4(a)) and remains constant at this value between 0.96 and at least 1.04 eV. For the 1 and 4 MeV data the shape of the spectrum is almost the same; these spectra rise and remain constant between 0.96 and at least 1.04 eV at a value of $(48\pm5)\times10^{19}$ cm^{-3} eV^{-1} (1 MeV) or $(43\pm5)\times10^{19}$ cm^{-3} eV^{-1} (4 meV). Therefore we can conclude that the defect activation energy spectrum of alkali-borosilicate glass does not seem to depend on the energy of the Xe ions.

The arguments described above indicate that the different behavior found for pure silica and alkali-borosilicate glass (as observed in Fig. 3.4) is not due to the difference in beam flux or energy, but must be due to the difference in glass compostion.

3.5 Conclusions

In conclusion, we determined the defect activation energy spectra and the temperature dependence of the radiation-induced viscosity for alkali-borosilicate glass under ion irradiation with 2 MeV Xe at a flux of $4\text{-}9\times10^{10}$ Xe/cm^2s. We compared these results with data for thermally grown SiO_2 films irradiated with 4 MeV Xe at a flux of 5×10^{12} Xe/cm^2s.

We find that defects in alkali-borosilicate glass are more stable than in pure silica. A binary collision model explains the shape of the obtained defect activation energy spectra. This contrasts with data for pure silica that were explained using a thermal spike model. In addition, the temperature dependence of the radiation-induced viscous flow in alkali-borosilicate glass deviates from a thermal spike behavior.

Relaxation measurements on thermally grown SiO_2 have also been performed after 2 MeV Xe irradiation at a flux of $1\text{-}1.5\times10^{11}$ Xe/cm^2s. The calculated time dependence of the stress changes using the universal spectrum after 4 MeV irradiation of thermal silica shows good agreement with the measured data after these 2 MeV irradiations. Moreover no beam flux dependency of the spectrum is found. In addition, the temperature dependence of the radiation-induced viscosity during 2 MeV irradiation of thermal silica also follows a thermal spike behavior. Finally, the defect activation energy spectrum of alkali-borosilicate glass does not seem to depend on the energy of the Xe ions. These arguments indicate that the difference in the nature of defect generation between pure silica and alkali-borosilicate glass must be due to the difference in glass compostion.

3.6 Aknowledgements

We aknowledge Jeroen Bakker (Utrecht University) for ERD measurements. This work is part of the research program of the Foundation for Fundamental Research on Matter (FOM) and was financially supported by the Dutch Organization for Scientific Research (NWO).

4. Anisotropic stress generation

4.1 Introduction

In chapter 3 we discussed the effect of defect annihilation on the average in-plane stress after ion irradiation. In this chapter we will focus our attention on a particular process occurring during ion implantation: 'anisotropic stress generation'.

As was discussed in chapter 3 the average in-plane stress during ion irradiation reaches an equilibrium. Stress saturation at a non-zero value indicates the presence of a continuous in-plane stress generating process [1]. This non-zero saturation stress results from a dynamic equilibrium between this anisotropic stress generating process and viscous flow that tries to relax the stress to zero. An example of this is shown in Fig. 3.2 which shows a positive saturation stress of ~32 Mpa for high fluence irradiation. In this chapter we will investigate the behavior of the anisotropic stress generating process as a function of sample temperature. Results are presented for the stress measurements performed on alkali-borosilicate glass and thermally grown silica during 2 MeV Xe ion irradiation (see section 3.2 for experimental details).

4.2 Theory and analysis

When an ion enters the solid it deposits its energy in atomic collisions and electronic stopping. As a result a sharp rise in the local temperature near the ion track occurs. For high irradiation energies the energy loss is mainly due to electronic stopping. Due to the low directional straggle the locally heated region around the ion track is more or less cylindrically shaped. Shear plastic relaxation of the local stress induced by thermal expansion of this hot cylindrical region results in a compressive in-plane stress on the material surrounding this region. If the material is not constrained by a substrate this can result in plastic deformation perpendicular to the direction of the ion beam. This process is called anisotropic growth. A more detailed study of this ion irradiation phenomenon is presented in chapter 5, where this process is used to deform micron-sized silica colloids.

If, however, the irradiated material is a thin film constrained by a substrate a compressive in-plane stress builds up. Stress saturation at a non-zero value results from a dynamic equilibrium between this anisotropic stress generating process and viscous flow that tries to relax the stress. For high fluences ($\phi \gtrsim 2\text{x}10^{13}$ Xe/cm^2 for 2 MeV Xe irradiation of alkali-borosilicate glass and thermally grown SiO_2 films) the average in-plane stress depends on the combined effect of viscous flow and anisotropic stress generation:

$$\frac{d\sigma}{d\phi} = Y_b \cdot \left(A - \frac{\sigma}{6\eta_{rad}} \right) , \tag{4.1}$$

with Y_b the biaxial stress state modulus of the film (ion modified region), A the in-plane strain generated per ion (anisotropic stress generation rate) and η_{rad} the radiation-induced viscosity. From Eq. (4.1) it follows that the in-plane stress exponentially reaches its saturation value $\sigma_{sat}=6A\eta_{rad}$. The anisotropic stress generation rate A can therefore be determined by fitting an exponential function to the high fluence part of the data (during ion irradiation).

4.3 Results and discussion

Figure 4.1 shows the temperature dependence of the anisotropic stress generation rate A during 2 MeV Xe ion irradiation of alkali-borosilicate glass at a flux of $4\text{-}9\times10^{10}$ ions/cm^{2}s (triangles). This value varies between $(7.4\pm1.3)\times10^{-17}$ cm^2/ion at 95 K and $(-3.5\pm1.1)\times10^{-18}$ cm^2/ion at 375 K. The decrease of the anisotropic stress generation rate with increasing temperature was also observed in [9, 12]. A possible explanation for this effect is that the in-plain strain generated by each thermal spike can be partly relaxed after the thermal spike phase. The plastically deformed region that is under compression due to the interaction between the thermal spike region and the surrounding material will try to relax to the state before ion impact. The rate at which this reverse relaxation process occurs depends on the thermal viscosity of the glass at a particular sample temperature. Hence this reverse relaxation rate will be higher at higher

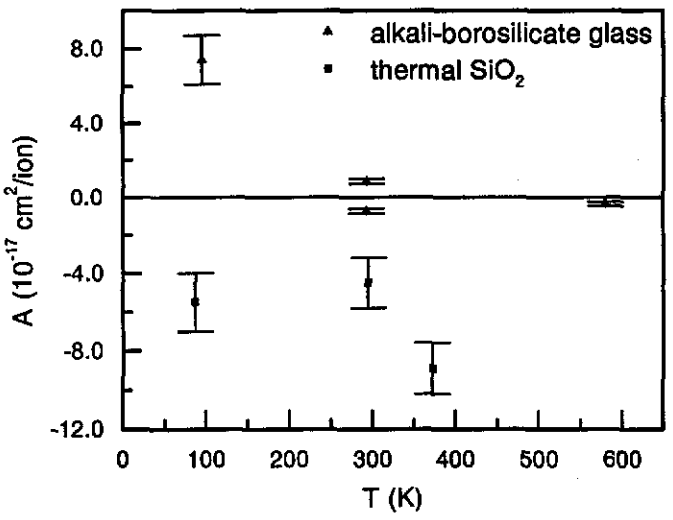

Figure 4.1 The temperature dependence of the anisotropic stress generation rate *A* during 2 MeV Xe ion irradiation of alkali-borosilicate glass (triangles) and thermally grown SiO_2 films on Si squares.

temperatures, resulting in effectively lower anisotropic stress generation rate *A*. As can be seen in Fig. 4.1 *A* becomes slightly negative for high temperatures. Indeed, the saturation stress for irradiation at 580 K remains tensile ($\sigma_{sat}<0$, see Fig 3.2).

Figure 4.1 also shows the stress generation rate during 2 MeV Xe ion irradiation of thermally grown silica at a flux of 1-1.5x10^{11} ions/cm^2s (squares). As can be seen the value of *A* is negative for all temperatures. By comparing these data with results for 4 MeV Xe ion irradiation of thermal SiO_2 presented in [12] where the value of *A* is positive up to ~ 500 K, we can conclude that the anisotropic stress generation rate *A* increases with increasing irradiation energy for all temperatures up to at least 375 K. This effect had already been observed in [1] at room temperature. More experiments need to be done to understand the physical origin of this negative value of the anisotropic stress generation rate. A possible explanation is given in [1]. Due to local heating near the ion track surface atoms are forced out of the material. The surrounding material then would attempt to fill the vacant space resulting in a net tensile stress.

4.4 Conclusions

We performed in-situ wafer curvature measurements to determine the temperature dependence of anisotropic stress generation rate during 2 MeV Xe ion irradiation of alkali-borosilicate glass and thermally grown silica. For alkali-borosilicate glass we observed a decrease in the deformation rate with increasing temperature and at high temperatures the rate becomes even slightly negative. This decrease might be due to the smaller thermal viscosity of the glass at higher temperatures. For thermally grown silica the value of the stress generation rate was negative for all temperatures. This should be contrasted with experiments in thermally grown silica using 4 MeV Xe that show a positive stress generation rate up to ~ 500 K. The anisotropic stress generation rate therefore increases with increasing irradiation energy.

In summary, the anisotropic stress generation rate is slightly negative at low irradiation energy, and positive at higher energies; the turn over energy depends on the type of glass used.

5. Colloidal spheroids with continuously variable shape*

5.1 Introduction

The synthesis of colloidal hard-sphere suspensions is a well explored and understood field of research. For example, silica spheres with core radii of up to a few hundred nanometers with very low polydispersity can be synthesized [16]. However, it is very difficult to synthesize colloidal particles with non-spherical shape. Oblate and prolate spheriods with low polydispersity would find numerous application in studies of self-assembly or in novel photonic materials [17, 18]. Ottewill et al. have been able to produce low yields of prolate particles by a molecular stretching technique [19], but monodisperse oblate spheroids have to our knowledge not been demonstrated.

In this chapter we combine our experience in colloidal chemistry [16] and ion beam modification of materials [1, 10] to synthesize a new class of ellipsoidal micro spheroids. From previous studies it is known that amorphous materials can undergo an anisotropic deformation under MeV heavy ion irradiation [3, 9]. In the past studies this effect was demonstrated by macroscopic expansion or by the build up of mechanical stress in irradiated thin films (see chapter 3, 4). In this report we apply this irradiation technique on micron sized colloidal silica with low polydispersity, to synthesize both oblate and prolate spheroids. The shape of these spheroids can be controlled by changing the irradiation conditions, and aspect ratios of at least 3.1 can be obtained.

5.2 Experimental

Two dispersions of silica spheres in ethanol, with different diameters, were synthesized using techniques described in Ref. [16]. They were dropped onto a clean surface of a Si(001) substrate, after which the ethanol was left to evaporate. Scanning electron microscopy (SEM) was used to view the spheres [20]. The two different sizes are easily distinguished with diameters sharply centered around 290 and 1030 nm and a dispersion of <2 %.

The particles were irradiated with 4 MeV Xe ions with the sample held at different angles with respect to the ion beam. The ion beam was electrostatically scanned to homogeneously irradiate the entire sample with a flux varying between 3 and 8×10^{10} ions/cm^{2}s. The projected mean ion range of 4 MeV Xe ions into silica is around 1.7 μm, well beyond the particle diameter. The base pressure during ion irradiation was 5×10^{-7} mbar. The Si substrate was tightly clamped against a temperature controlled copper sample stage cooled to about 90 K using liquified nitrogen. The samples were irradiated to different fluences between 3×10^{13} and 8×10^{14} Xe/cm^2 at a beam flux of about 6×10^{10} Xe/cm^{2}s. In addition, irradiations were performed using a 500 keV Xe ion beam with a flux of ~ 6.5×10^{12} Xe/cm^{2}s.

5.3 Results and discussion

In Fig. 5.1(a) a SEM image is shown of the silica spheres on the Si surface, viewed under normal incidence to the substrate. The two sizes are easily distinguished. The diameters are sharply centered around 290 and 1030 nm.

Next, the particles were irradiated with 4 MeV Xe ions with the sample held at an angle of +45° with respect to the direction of the ion beam, as indicated in the schematic inset in Fig. 5.1. Figures 5.1 (b),(c) and (d) show SEM images taken after irradiation to a fluence of 3×10^{14} ions/cm^2. The images were obtained using different sample-tilt angles in the microscope. The three (almost) orthogonal projections provide a full identification of the particle shape after irradiation: a biaxial expansion is observed in the plane normal to the direction of the ion beam, while a contraction is observed in the beam direction. In Fig. 5.1 (b) these oblate spheroids are viewed along the direction of the ion beam, i.e. at a +45° tilt angle as indicated in the schematic inset. In this particular projection, the spheroids appear circular. The dashed circle represents the circumference of unirradiated spheres. The diameters of both the large and small particles have increased by 24 %. The two images perpendicular to the ion beam, Figs. 5.1 (c) and (d),

* This chapter is based on an excerpt from: E. Snoeks, A. van Blaaderen, C.M. van Kats, M.L. Brongersma, T. van Dillen and A. Polman, submitted to Science

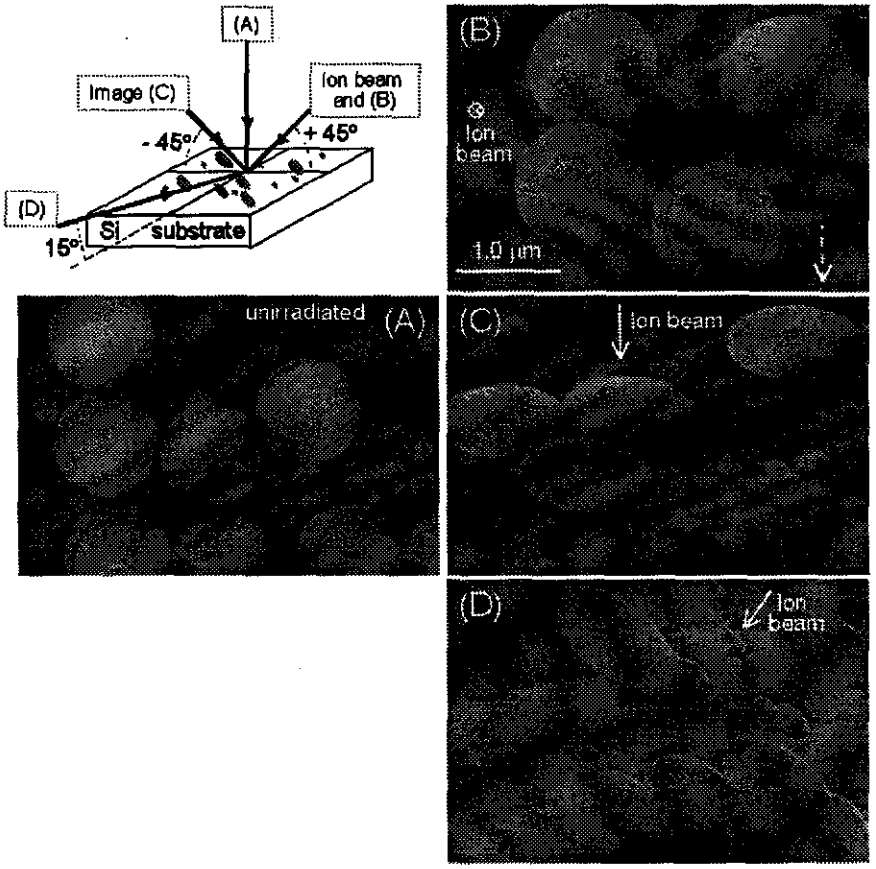

Figure 5.1 Scanning electron microscopy (SEM) images of two sizes of silica particles on a silicon substrate. (A) is a top view (*0°-tilt*) *of the spheres as grown. (B, C, D) show spheroids after* 4 *MeV Xe* irradiation to a fluence of 3×10^{14} /cm^2, imaged under the different view angles that are indicated in the schematic inset. The dashed arrow in (B) indicates the direction of a subsequent irradiation performed to obtain the prolate particles.

show the elliptically shaped side views of the spheroids. The size decrease of the deformed particles along the direction of the ion beam with respect to the original diameter is 35 %.

The images of Fig. 5.1 unambiguously show that anisotropic plastic deformation occurs: the silica biaxially expands transverse to the direction of the ion beam, while it uni-axially contracts in the direction along the ion beam. The volume of the spheroids remains almost unchanged.

Experiments as described above were performed for various Xe ion fluences ranging from 3×10^{13} to 8×10^{14} ions/cm^2. Figure 5.2 shows the average transverse (circles) and parallel (dots) diameters of the oblate spheroids as a function of fluence, for the large (Fig. 5.2 (a)) and small (Fig. 5.2 (b)) particles. The magnitude of the deformation follows a clear monotonous trend, and the aspect ratio of the strongest deformed spheroids in Fig. 5.2 is 3.11±0.13. The drawn line is a linear fit through the transverse axis data, while the dashed line is calculated from the drawn line assuming constant volume. Both lines describe the data quite well, *indicating that the volume of the particles does not significantly change during the* deformation process. The lines shown in Fig 5.2 (a) and (b) for the large and small particles are identical and only scaled by the ratio of the original sphere diameters. As can be seen, the large spheres change shape in the same way as the small spheres do.

The particles shown so far have all been obtained using 4 MeV Xe ion irradiation at 90 K. We have also studied beam-induced deformation of silica spheres at room temperature. The particles deform in the same way but a 4.2±1.0 times higher fluence is required than at 90 K to obtain the same amount of deformation. This agrees well with measurements of the temperature dependence of the deformation rate on planar silica films [12].

As was explained in section 4.2, the anisotropic deformation phenomenon can be described by a microscopic thermal spike model in which cylindrically shaped narrow thermal spike evolves around the

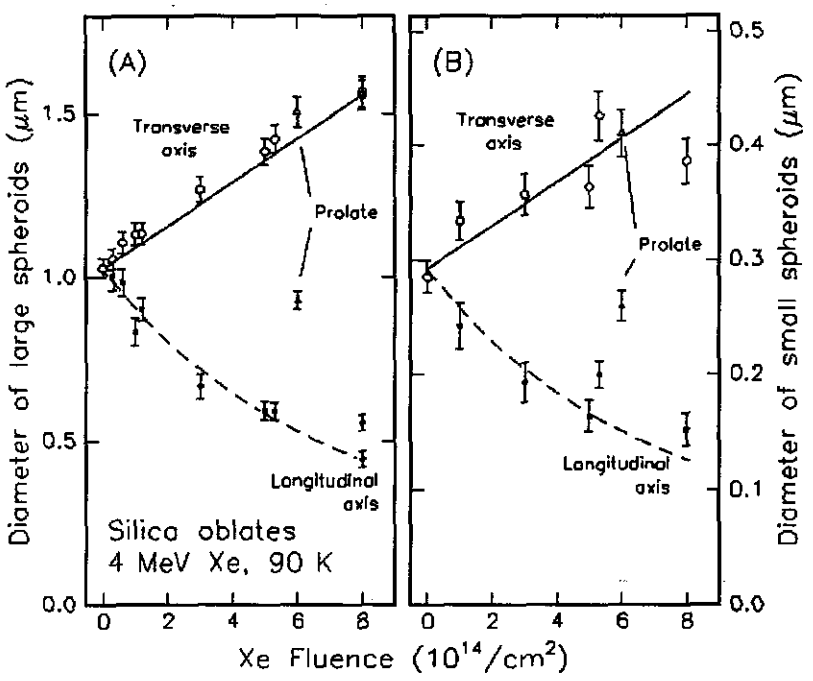

Figure 5.2 Diameter transverse to (open data marks) and along the direction of the ion beam (solid marks) for the (A) large and (B) the small spheres. Round marks correspond to oblate spheroids, and triangles to prolate spheroids.

ion track, provided that the electronic energy deposition (~2 keV/nm for 4 MeV Xe) is high enough. The observed macroscopic deformation would be the result of the integrated effect of a large number of microscopic single ion events. Note that at a fluence of 7×10^{14} ions/cm^2 each micron-sized particle has been impacted by some 10^7 Xe ions. Any statistical deviations are therefore expected to average out over such large numbers, so that the particles are expected to be very monodispersive in both size and shape.

To prove that the deformation is indeed the result of the anisotropic nature of the thermal spike around each ion track at 4 MeV, experiments were also performed using 500 keV Xe ions [21]. The amount of stopping is roughly equal to the case of 4 MeV (~ 2 keV/nm), but in this case nuclear collisions dominate the energy depostion. This leads to a more spherically shaped excitated region embedded in the solid, so mostly radial pressure will build up without shear components. Although the energy deposition in such a region could be high enough for strong thermal expansion, no anisotropy would be observed. Indeed, we did not observe the plastic shape change after irradiation at an energy of 500 keV, even to a fluence as high as 1×10^{16}/cm^2.

Finally we will demonstrate how the irradiation technique can be used for synthesis of prolate spheroids. First oblate particles were made, using 4 MeV Xe to a fluence of 3×10^{14} Xe/cm^2, precisely as shown and explained in Fig. 5.1. Next the particles were irradiated with 4 MeV Xe ions to the same fluence of 3×10^{14} Xe/cm^2, with the sample tilted at -45°, i.e. orthogonal to the direction of the first irradiation. This is indicated by the dashed arrow in Fig. 5.1 (b). Figure 5.3 shows the SEM image of these doubly irradiated particles. The particles in Fig. 5.3 (a), taken using the same sample orientation as in Fig. 5.1 (b), now appear elliptical. This is true for all tilt angles within the plane expanded by the two ion beam directions. Figure 5.3 (b) shows the same sample, imaged in a direction that is almost normal to both of the two ion beam directions (75° off of the surface normal). From this angle of view the particle projection is close to circular: the spheroids in Fig. 5 are thus indeed prolate shaped. The total ion fluence used to form these prolate spheroids was 6×10^{14}/cm^2, and the relative dimensions of the particles are also included in Fig. 5.2 (triangles). Note that the dimensional change perpendicular to both the ion beams (the transverse axis) falls close to the trend observed for the transverse length change of the oblate spheroids. This further confirms that the deformation phenomenon is beam-directionally anisotropic, and that a high level of shape control

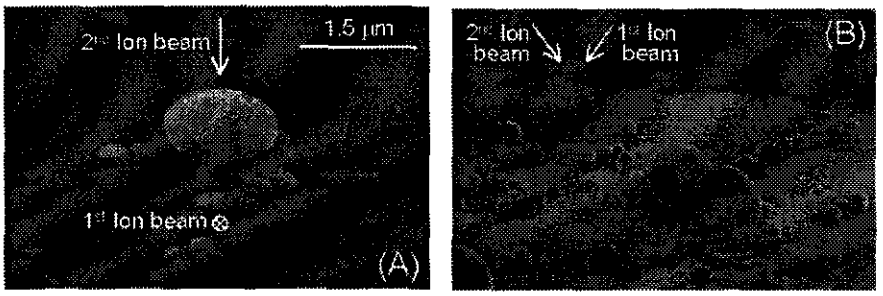

Figure 5.3 SEM images of silica particles such as shown in Fig. 5.1 after an additional orthogonal Xe ion irradiation to a fluence of $3\times10^{14}/cm^2$. (A) is viewed along the direction of the first ion irradiation (+45° tilt), and (B) almost perpendicular to both ion beams. (15° tilt from the sample surface, 90° azimuth.)

can be achieved.

It is interesting to note that, while a linear increase in the transverse diameter of the spheroids is observed in Fig. 5.2, an exponential growth of the transverse lengths with fluence would be expected if the deformation rate is constant. That this is not observed implies that the apparent deformation rate per ion decreases with ion fluence. One explanation for this effect could be that the increasing surface curvature or surface-to-volume ratio combined with surface tension makes it less favorable to deform stronger for higher fluences. However, the fact that the small spheres deform in exactly the same way as the large spheres in this experiment, excludes this possibility. Alternatively it may be that the actual deformation rate A decreases due to a structural or compositional change of the silica during ion irradiation. To describe the data in Fig. 2 we find that the strain rate per ion would gradually decrease from 6.5×10^{-16} cm^2/ion to 4.3×10^{-16} cm^2/ion.

5.4 Conclusions

We use 4 MeV Xe ion irradiation to deform two sizes of silica colloid spheres (diameter: 290 nm and 1030 nm) produced by chemical synthesis. At a temperature of 90 K we observe a bi-axial expansion transverse to the direction of the ion beam and a uni-axial contraction along the direction of the ion beam. The transverse dimension increases linearly with ion fluence and the volume of the oblates remains almost unchanged. An aspect ratio of 3.11 ± 0.13 is achieved after a fluence of 8×10^{14} Xe/cm^2. The small spheres deform in exactly the same way as the large spheres. A 4.2 ± 1.0 times higher fluence is required to obtain the same deformation at room temperature. No anisotropic plastic deformation was found using 500 keV Xe ions, indicating that the observed deformation is the result is the result of the anisotropic nature of the thermal spike around the ion track.

Finally, we produced prolate spheroids after two successive 4 MeV Xe ion irradiations (at 90 K). The direction of the second ion beam was perpendicular with respect to the direction of the first irradiation. and the same fluence was used for both irradiations. We can therefore control the shape of silica spheroids at a high level of accuracy..

6. References

[1] E. Snoeks, T. Weber, A. Cacciato and A. Polman, J. Appl. Phys. **78** (7), 4723 (1995)
[2] R.A.B. Devine, Nucl. Inst. Meth. B **91**, 378 (1994)
[3] S. Klaumünzer, Radiat. Eff. Def. in Sol. **110**, 79 (1989)
[4] M. Ohring, The materials science of thin films (Academic Press, Inc.)
[5] P.A. Flinn, D.S. Gardner, and W.D. Nix, Trans. Electron Devices ED-34 (3), 689 (1987)
[6] C.A. Volkert, J. Appl. Phys. **70** (7), 3521 (1991)
[7] A. Polman, C.A. Volkert, 'manual wafer curvature'
[8] M.L. Brongersma, E. Snoeks and A. Polman, Appl. Phys. Lett. **71** (12), 1628 (1997)
[9] A. Benyagoub, S. Löffler, M. Rammensee, S. Klaumünzer and G. Saemann-Ischenko, Nucl. Inst. Meth B **65**, 228 (1992)
[10] E. Snoeks, A. Polman and C.A. Volkert, Appl. Phys. Lett. **65** (19), 2487 (1994)
[11] D.L. Griscom, G.H. Sigel, Jr., and R.J. Ginther, J. Appl. Phys. **47**, 960 (1976)
[12] M.L. Brongersma, 'Optical properties of ion beam synthesized Si nanocrystals in SiO_2', Ph.D.-thesis, Utrecht University (1998), ch. 2,3, M.L. Brongersma, E. Snoeks, T. van Dillen, and A. Polman, submitted to J. Appl. Phys.
[13] Some stress measurements (at certain temperatures between 95 and 580 K) were performed on the same sample using a procedure consisting of: stabilizing the temperature, ion irradiation to equilibrium stress and measuring the stress after switching off the ion beam.
[14] G.H. Vineyard, Rad. Eff. **29**, 245 (1976)
[15] E. Snoeks, P.G. Kik and A. Polman, Optical Materials **5**, 159 (1996)
[16] A. van Blaaderen and A. Vrij, *Langmuir* **8**, 2921 (1993).
[17] L. Onsager, *Ann. (N.Y.) Acad. Sci.* **51**, 627 (1949)
[18] D. Frenkel and B. M. Mulder, *Mol. Phys. 55*, 1171 (1985).
[19] C.C. Ho, A. Keller, J. A. Odell, R. H. Ottewill, Colliod Polym. Sci. **271**, 469 (1993)
[20] Philips *XL3O FEG* operated at 10 kV.
[21] Here only the smaller particles (with 290 nm diameter)were used because the ion range of 500 keV Xe in silica is about 250 nm.

Appendix A. Theory of isothermal uni-molecular defect annealing

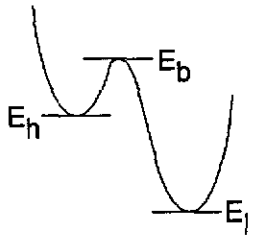

Figure A.1 Schematic illustration of a double well potential

In this appendix we will summarize the theory of uni-molecular defect annealing, described in Refs. [1] and [2.]

Defect annealing is described by considering an array of isolated double well potentials as depicted in Fig. A.1. A defect is considered to be in the higher energy minimum of the potential (at energy E_h). Defect annihilation occurs when the local structure jumps to the lower energy level E_l, thereby passing the energy barrier E_b. The energy needed for this jump (annihilation) is equal to E_b - E_h, the activation energy Q.

Defect annealing is described by a differential equation:

$$-\frac{dq}{dt} = c \cdot q^n \,, \tag{A.1}$$

where q is the concentration of defects, t is the time, c is the reaction constant and n is the order of the reaction. In this chapter we will only consider the case of uni-molecular defect annealing where the order n of the reaction is unity. The reaction constant c can be equated to an Arrhenius expression with an activation energy Q:

$$c = \nu_0 \cdot e^{-\frac{Q}{kT}} \,, \tag{A.2}$$

where ν_0 is an attempt frequency [3], k is Bolzmann's constant and T is the temperature. The attempt frequency ν_0 is assumed to be kT/h, where h is Planck's constant. When the temperature remains constant (isothermal annealing) the solution of Eq. (A.1) is given by:

$$q(t;Q) = q_0(Q) \cdot e^{-\frac{t}{\tau(Q)}} \,, \tag{A.3}$$

where $q_0(Q)$ is the value of q at t=0 and $\tau(Q)$ the characteristic annealing time for a defect with activation energy Q, given by:

$$\tau(Q) = \frac{1}{c} = \frac{h}{kT} \cdot e^{\frac{Q}{kT}} \,. \tag{A.4}$$

The exponential in Eq. (A.3) is the characteristic annealing function $\Theta_1(Q,t)$ for uni-molecular defect annealing. The behavior of the characteristic annealing function is shown in Fig. A.2 as a function of Q for a fixed time t. The point of inflection [4] is called the characteristic activation energy Q_t, given by:

$$Q_t = kT \cdot \ln[t \cdot kT / h] \,. \tag{A.5}$$

Fig. A.3 shows $\Theta_1(Q,t)$ as a function of t for various energies Q.

The concentration of defects is probed by the measurement of a physical quantity, say P, e.g. a change in density associated with the annihilation of the defects. Then:

$$P(t) = \int_0^\infty p_0(Q) \cdot \Theta_1(Q,t) dQ \,. \tag{A.6}$$

The mathematical description of Eq. (A.6) is that a function $P(t)$ is built up of a combination of functions $\Theta_1(Q,t)$ as indicated in figure A.3. The function $p_0(Q)$ is a weight function which determines the eventual contribution to the value of P due to the annealing of defects with activation energy Q.

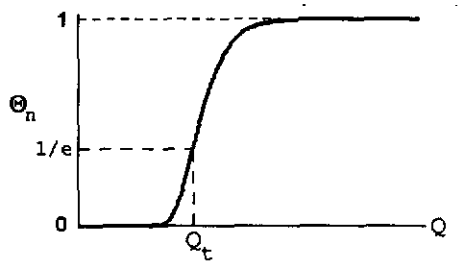

Figure A.2 The characteristic annealing function for isothermal uni-molecular defect annealing

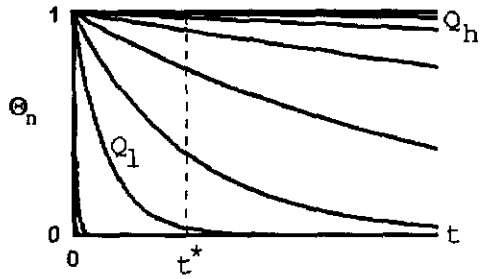

Figure A.3 Characteristic annealing functions versus the time t for several defects with activation energie Q.

The time derivative of the property P is called the 'rate of annealing'. At a certain time t^* this rate is only determined by defects with activation energies in the range between Q_l en Q_h, as can be seen in Fig. A.3. Defects with activation energies smaller than Q_l have already been annealed out and defects with activation energies higher than Q_h will anneal out on larger time scales. This indicates that at a certain time only defects will anneal out that have activation energies in a small band (about 6 kT).
The rate of annealing is given by:

$$-\frac{dP}{dt} = \int_0^\infty p_0(Q) \cdot \left[-\frac{d\Theta_1}{dt} \right] dQ \,. \qquad \text{(A.7)}$$

This means that defects annihilating simultaneously at the maximum of $d\Theta_l/dt$ have a maximum contribution if we neglect the effect of the initial activation energy spectrum $p_0(Q)$. For isothermal annealing $d\Theta_l/dt$ is proportional to $d\Theta_l/dQ$ (as a function of Q). Hence, defects annihilating simultaneously mainly consist of defects possessing the characteristic activation energy Q_t.

The main concern of defect annealing measurements in this report is to determine the activation energy spectrum $p_0(Q)$ from the data $P(t)$. The inversion of the isothermal annealing data $P(t)$ to extract $p_0(Q)$ can be done by means of a Laplace transform. If, however, the spectrum $p_0(Q)$ is very broad, many times kT, the characteristic annealing function (Fig. A.2) may be approximated by a step function. In that case (A.7) reduces to:

$$p_0(Q_t) \cong -\frac{t}{kT} \cdot \frac{dP}{dt} = -\frac{dP}{dQ_t} \,. \qquad \text{(A.8)}$$

In conclusion, at a time t defects are annealing that have activation energies which lie in a narrow band (order 6 kT) around the characteristic annealing energy Q_t, given by Eq. (A.5). To extract the initial activation energy spectrum $p_0(Q)$ from the data $P(t)$ we can make an approximation using Eq. (A.8). These equations will be used to analyse our data in this report. A more detailed study of defect annealing is described in Refs. [1, 2].

References and notes

[1] M.R.J. Gibbs, J.E. Evetts, J.A. Leake, J. Mat. Science **18**, 218 (1983)
[2] W. Primak, Phys. Rev. **100** (6), 1677 (1976)
[3] The frequency ν_0 is the number of attempts per second to pass the energy barrier (Fig. A.1). We assume that this frequency depends on the temperature since the thermal energy increases with increasing temperature.
[4] The point of inflection is found by solving $d^2\Theta/dQ^2 = 0$.

Appendix B. Abstract for the 11th International Conference on Ion Beam Modification of Materials, August 31 – September 4, 1998, Amsterdam, The Netherlands

DETERMINATION OF ACTIVATION ENERGY SPECTRA FOR ANNEALING OF ION RADIATION INDUCED DEFECTS IN SILICA GLASSES

T. van Dillen, E. Snoeks, M.L. Brongersma, and A. Polman, FOM-Institute for Atomic and Molecular Physics, Amsterdam, The Netherlands.

Little is known about the defect activation energy spectra of ion irradiation induced defects in glasses. In this work we measure the sample curvature using a sensitive scanning-laser technique to detect small changes in mechanical stress in the irradiated surface layer of a glass during and after irradiation.
Borosilicate glass slides were irradiated at 2 MeV Xe at temperatures between 95 and 590 K. During ion irradiation, stress changes occur due to structural transformations, radiation-induced viscous flow, an anisotropic stress generating effect and the creation/annihilation of point defects. The beam-induced stress changes saturate after a typical fluence of $4x10^{13}$ Xe-ions/cm^2.
After switching off the ion beam the stress changes towards tensile values on time scales varying from seconds to several days. This is attributed to the annealing of volume occupying point defects, which is governed by a broad spectrum of activation energies. When the ion beam is switched on again, the stress returns to its original value within typically $5x10^{12}$ Xe-ions/cm^2.
Annealing of defects is observed for all temperatures, indicating contributions to the activation energy spectrum between 0.2 and 1.9 eV. The shape of the spectrum strongly depends on the irradiation temperature.
These results contrast to what was found for thermally grown SiO_2 films on Si. For pure SiO_2 the spectrum is independent of irradiation temperature and only has contributions up to 0.7 eV.
The difference may be caused by the presence of the boron, which is known to stabilize irradiation induced defects in the silica network.

Contact Author:

Name:	T. van Dillen
Organization:	FOM-Institute for Atomic and Molecular Physics
Group:	Opto-electronic materials
Address:	Kruislaan 407
ZIP/City:	1098 SJ Amsterdam
Country:	The Netherlands
Phone:	+31 20 6081234
FAX:	+31 20 6684106
e-mail:	dillen@amolf.nl